# Ground Segment Design for Broadband Geostationary Satellite With Optical Feeder Link

Sylvain Poulenard, Michael Crosnier, and Angélique Rissons

***Abstract*—High-data-rate space-to-ground optical links are anticipated to be an alternative to radio-frequency spectrum congestion for the next generation of high-throughput geostationary satellites. An affordable site diversity system based on several optical ground stations (OGSs) and an optical fiber network is necessary to overcome cloud obstruction of the feeder link. In this paper, we report three promising sets of OGSs in the vicinity of existing ingress and egress points of a selected pan-European optical fiber network. These OGS networks are optimized for reaching at least 99.9% feeder link availability while minimizing the overall cost of the system. For the first time, the optical fiber network between OGSs is optimized using existing high-data-rate fiber links to limit its expense. The resulting cost estimates for each OGS network highlight the need to define a new cost model considering optical feeder link specificity. In addition, the link availability is simulated using a 2 year cloud mask data bank, taking into consideration practical cloud blockage forecasting duration and assuming optical transmission through thin ice clouds.**

***Index Terms*—Feeder link; Optical ground station network; Satellite system availability; Space-to-ground optical links.**

## I. Introduction

The next generation of broadband satellite communication systems will play a key role in reliably delivering more than 30 Mbps to all European households by 2020, meeting the objectives of the European Commission [1]. Based on market analysis [2], the targeted capacity of next-generation high-throughput satellites should reach 1 Tbit/s, which is one order of magnitude higher than what is currently provided by state-of-the-art satellites (e.g., Ka-Sat or Viasat 1). For such capacity, recent system studies [3,4] demonstrated that at least 30 Q/V band gateways spread over Europe are necessary to provide connection between the Earth and the satellite, the so-called feeder link. This increases the complexity of the frequency coordination that aims to control the intersystem interference. In 2009, a terabit/second free-space optical link at 1.55 μm was demonstrated for the first time between the roofs of two buildings [5], reinforcing the concept of the optical feeder link as an alternative solution to radio frequencies. Compared to radio frequency (RF) solutions, optical communications have the advantage of very-low-divergence beams, ~1 km for a terabits/second link, avoiding interference and thus frequency coordination. On the other hand, optical beams suffer from distortion by atmospheric turbulence and obstruction by most of the clouds. Here, we focus on cloud obstruction only, and we assume that atmospheric turbulence does not impact the system availability. As depicted in Fig. 1, the obstruction of the optical signal by clouds [6] necessitates the design of a network of geographically distant optical ground stations (OGSs) to reach the typical link availability of 99.9% required by satellite operators [3,4]. We call this network the optical ground station network (OGSN). Researchers have already focused on OGS positioning to satisfy optical link availability for deep-space communications [7], Earth observation [8,9], and broadband telecommunications [10,11]. Nevertheless, in these studies, the OGS positioning was optimized only for optimum weather conditions and did not consider the satellite operator backbone cost. The latter is of the most importance for a broadband satellite system, as it corresponds to a great portion of the overall system cost. In fact, the main current obstacle to convincing satellite operators of the feasibility of a terabit/second optical feeder link is the cost of its ground segment.

Therefore, the main goals of this article are as follows:

- To propose and apply a new method for OGS positioning, taking into consideration the cost of the connection to real high-data-rate fiber networks.
- To simulate the performance of the optimized OGSNs during two full years, 2010–2011, considering a realistic cloud forecasting capability and a practical OGSN concept of operation.
- To address for the first time the optimization of the ground segment network topology for cost reduction of the satellite operator backbone with a terabit/second optical feeder link. The backbone cost is derived in the frame of the research project “Broadband Access via integrated Terrestrial and Satellite systems (BATS)” [11]. BATS addresses the delivery of broadband Internet to

Manuscript received September 24, 2014; revised January 15, 2015; accepted January 20, 2015; published March 31, 2015 (Doc. ID 223727).

S. Poulenard is with Airbus Defence and Space in partnership with Institut Supérieur de l’Aéronautique et de l’Espace, Toulouse, France (e-mail: sylvain.poulenard@astrium.eads.net).

M. Crosnier is with Airbus Defence and Space, Toulouse, France.

A. Rissons is with Institut Superieur de l’Aeronautique et de l’Espace, Toulouse, France.

http://dx.doi.org/10.1364/JOCN.7.000325

 

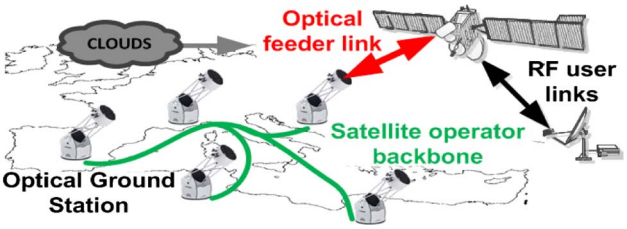


Fig. 1. Schema of an optical feeder link system for a broadband geostationary satellite. Ground segment includes OGS positioning as well as link optimization of the satellite operator backbone.

underserved areas in Europe through multiple access network connections (mobile, fixed, and satellite).

This article is divided into five sections, of which Section I is the introduction. In Section II, the positioning of the OGSs is optimized according to the link budget constraints as well as the connectivity constraints to existing optical fiber networks (step 1). In Section III, the backbone is optimized to be more cost effective (step 2) for the specific case of BATS. In Section IV, the concept of operation of the OGS network is defined. In Section V, we simulate the performance of optimized OGSNs during the two full years 2010–2011, taking into account a realistic cloud forecasting capability. Sections II–V are indicated in the flowchart given in Fig. 2. Finally, Section VI concludes the paper.

## II. Optical Ground Station Positioning

The typical availability required by the satellite operators for the feeder link is 99.9% [3,4]. An availability of 99.7% will also be analyzed here as an opportunity to decrease the number of OGSs, and therefore the overall system cost, while still providing an acceptable end-user quality of experience. Satellite operators have specified both availability targets.

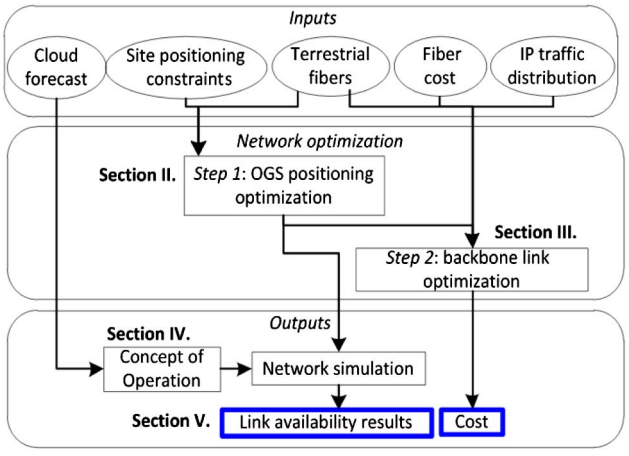


Fig. 2. Flow chart depicting the calculation steps for the evaluation of optical feeder link system performance and backbone costs. The sections of the paper describing those steps are also indicated.

### A. Methodology

In the literature, the OGS sites are selected either within a pool of zones [7,8,12] or from a list of punctual locations [6,9]. Despite the fact that the former approach is more demanding in computational resources, it is expected to provide a more optimized network, making it the approach of choice in this study. Within these zones, the optimization of the OGS network can be performed either by testing the link availability results for all possible combinations [7] or by an iterative greedy optimization process based on conditional opposite weather conditions [12]. The latter was implemented because it reduces the computation time; it consists of the following steps:

- Defining the zones of interest (see Fig. 4 below).
- Selecting the initial site: the site with the highest probability of a cloud-free line of sight (CFLOS).
- Selecting the other sites $OGS_i$ with an iterative process for $i \in [2{:}\infty]$: At every step $i$, $OGS_i$ is the site that maximizes the probability of a CFLOS when no site is available in the $(i-1)$-OGSN. From the estimate of the $(i)$-OGSN feeder link availability, the loop is either continued if the targeted availability is not reached or stopped. In the latter case, the $N$-OGSN refers to the optimized OGS of $N$ OGSs.

### B. Cloud Mask Data Base

The Spinning Enhanced Visible and Infrared Imager (SEVIRI) is a multiple-channel imager installed on the Meteosat Second Generation (MSG) satellite located at 0.5° west in geostationary orbit [13]. SEVIRI scans the Earth disk from south to north in 12.37 min, providing 12 spectrally filtered images. These images are collected and processed by the Satellite Application Facility—Nowcasting and Very Short Range Forecasting (SAF-NWC) to derive one cloud mask every 15 min. The SAF-NWC cloud mask data base provides the best trade-off between temporal (15 min) and spatial (~4 km) resolutions currently available. In addition, a geostationary satellite covering Europe would be located fairly close to the 0.5° west MSG satellite. Therefore, the cloud mask can be directly used for link availability estimation over Europe and Africa, without the need for image warping against parallax errors. Then the type of cloud corresponding to each image pixel is identified in this data base using the cloud type algorithm [14] based on multispectral thresholding on brightness temperature and reflectance. These clouds are classified among 20 types, and their respective optical attenuation at a 1.55 μm wavelength has been deduced in a recent study [15]. It was found that the attenuation of a high-altitude thin cirrus cloud (ice cloud) is less than 5.4 dB, taking into consideration statistical uncertainty. On the other hand, all the other types of clouds obstruct the optical signal. Figure 3 illustrates one of these cloud masks after projection on a grid of 3.8 km × 3.8 km. A total of 100 GB of data has been considered here, corresponding

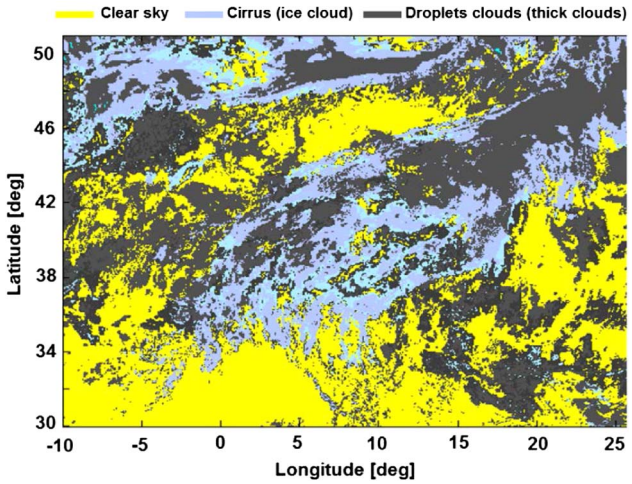


Fig. 3. Cloud mask showing the areas over Europe where the optical link can either be unobstructed (clear sky), partly attenuated (cirrus), or totally obstructed (droplets cloud).

to the imaging of Europe and North Africa over a period of 2 years with a temporal resolution of 15 min.

### *C. Scenarios, Zones of Interest, and the Pan-European Network*

The zones of interest for the OGS positioning optimization are deduced from the constraints of two domains: the link budget and the cost of the backbone. Considering the former domain, the elevation angle toward the satellite shall be over 30° for the implementation of mitigation techniques against atmospheric turbulence [16]. It is assumed that these techniques make the system availability independent of atmospheric turbulence.

Also, the OGSs should be localized close to a high-data-rate optical fiber network. The low-cost pan-European network has been chosen to handle the satellite operator backbone network; it is a virtual backbone formed by various operators that transfer data all over Europe and Turkey. The ingress and egress points of this pan-European network are called points of presence (PoPs). They are either public entry points like an Internet exchange point [17] or the private PoPs of three main terrestrial wholesale carriers (Level 3 [18], Cogent [19], and Interoute [20]). In addition, the PoPs of five submarine cables [21] (SeaMeWe-5, AAE-1, TE North/TGN-Eurasia/SEACOM/Alexandros, IMEWE, and SeaMeWe-4) that will comply in 2020 with a terabit/second capacity were added to widen the geographic extension of the zones of interest. The resulting combined network is the extended pan-European network.

In our study, a zone of interest corresponds to an area around the connection points to the networks defined above. On one hand, larger zones of interest lead to smaller numbers of OGSs to meet a given link availability. On the other hand, the longer the segment between the OGS and the PoP, the higher the price. As no commercial offer currently exists for this 1 TB/s link, it shall be deployed. The profitability of deploying it is out of the scope of this study, but the price information provided by the terrestrial network operator encourages limiting its length. Table I presents the results of five preliminary optimization runs carried out to estimate the sensitivity of the OGSN size with respect to the radius of the zones of interest around the PoPs of the pan-European network. For a targeted link availability of 99.9%, 9 OGSs are required if no constraints are imposed on the OGS-to-PoP length, while up to 14 are necessary if the radius of the zones of interest is limited to 50 km. Moreover, a link availability of 99.9% could not be reached at a radius shorter than 25 km. Note that the sensitivity is lower for reduced required link availability.

Based on these results, the zones of interest are assumed to have a 50 km radius in the rest of the study, ensuring the convergence of the optimization with limiting the expense of the OGS-to-PoP segment.

Eventually, the OGSN optimization has been performed for four system scenarios (SYS), illustrated in Fig. 4. In SYS 0 a reduced number of PoPs in the pan-European network were selected from the cheapest optical fibers. In SYS 2 all the PoPs of the pan-European network are considered. Finally, SYS 1 and SYS 3 correspond to SYS 0 and SYS 2, respectively, assuming that the link availability gains offered by Africa and the Middle East are accessible due to the submarine cables stated previously. SYS 3 consists of the all the PoPs of the extended pan-European network.

In order to decrease the OGSN size, we decided to allocate 5.4 dB in the link budget for transmission through thin cirrus. Such attenuation can be reasonably overcome due to high-power optical sources. This choice is also reinforced by the rise in cirrus occurrence in the European mid-latitude [22] and their great spatial extent.

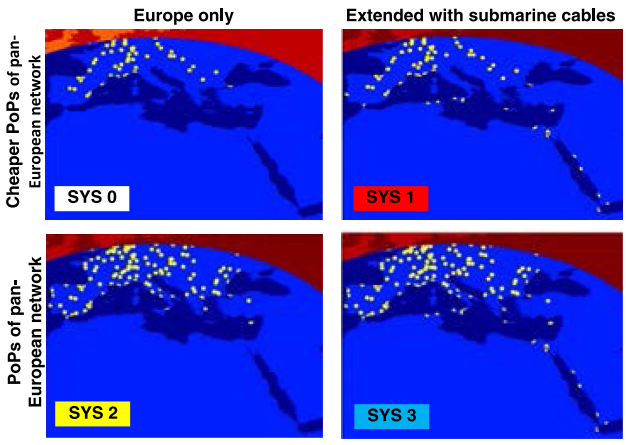


Fig. 4. Zones of interest (shown by the 50 km radius yellow dots) used for the OGS site research. The red area is excluded because the elevation angle to the satellite is below 30° (e.g., 13°E orbital position). SYS 0 consists of the most used PoPs in the pan-European network. SYS 1 is the extension of SYS 0 in Africa and the Middle East through the use of submarine cables. SYS 2 corresponds to all the PoPs of the pan-European network. SYS 3 consists of all the PoPs of the extended pan-European network.

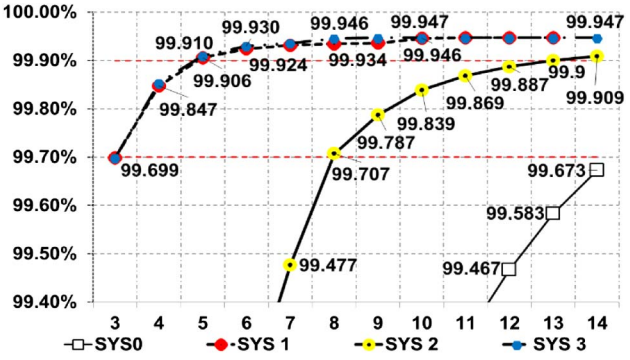


Fig. 5. Optical ground station network size as a function of the feeder link availability and the zones of interest.

### D. Results

Figure 5 provides, for the four scenarios (SYS 0/1/2/3), the sensitivity of the OGSN size as a function of the required feeder link availability. Tables II–IV provide the exact locations of the optimized OGS selected at each iteration for the three system scenario 1/2/3. As expected, the last remaining percentage of availability is more demanding in terms of the number of OGSs, which encourages us to study new types of broadband services with lower-level availability. For a first assignment, satellite operators specified 99.7% as a reasonable value for optical feeder link availability. Considering all the PoPs of the pan-European network (SYS 2), it is seen that the numbers of sites are 14 and 9, respectively, for feeder link availabilities of 99.9% and 99.7%. The size of these networks could be diminished by increasing the bearable distance between the PoP and the OGS, as in Table I. It is also shown that the pool of potential PoPs cannot be too restricted (as in SYS 0), in order to keep small the number of sites in the network. It also turns out that three sites (Zafarana, Yanbu, and Jeddah) in the African and Middle East sites are sufficient to reach a 99.7% link availability over a year. Starting from these latter three sites, a 99.9% link availability is reached with two more sites in Europe (Gibraltar and Montpellier for SYS 1; Sevilla and Grenoble for SYS 3).

The three optimized OGSNs with 99.9% optical link availability for SYS 1, SYS 2, and SYS 3 are depicted in Fig. 6. SYS 0 is discarded for the rest of the study due to its high number of sites, so it is not in the illustration.

## III. Satellite Operator Backbone Optimization

In this section, we optimize the satellite backbone to limit its cost for the specific case of the BATS project [11]. The three optimized OGSNs (SYS 1/SYS 2/SYS 3) designed in the previous section are inputs for this optimization.

### A. BATS Project Description and Assumptions

The BATS project addresses the delivery of future broadband Internet services in “unserved” and “underserved” areas in Europe. As depicted in Fig. 7, the innovating hybrid BATS operator manages multiple access network connections (mobile, fixed, and satellite) with two main entities: the integrated network gateway (ING) and the intelligent user gateway (IUG). An IUG is similar to an Internet box that provides access to three networks: a national fixed provider, a national mobile provider, and a European satellite provider.

An ING monitors and controls several IUGs; it routes the traffic depending on link status, the type of application, and the required quality of experience. All the flows from/to an IUG converge to its serving ING. The ING is therefore a central entity for all flows of the corresponding country. The BATS operator serves 28 European countries. In our approach, there is only one ING per country, as illustrated in Fig. 7. In this context, the BATS backbone is necessary to route all the flows between the OGSs and the 28 INGs. All the OGSs should handle 1 Tbit/s, which must be distributed to all the INGs depending on the user locations. The

TABLE I
Number of OGSs as a Function of OGS-to-PoP Maximal Distance

| Radius of Zone of Interest (km) | $N$ at 99.7% | $N$ at 99.9% |
|---|---|---|
| ∞ | 6–7 | 9 |
| 200 | 8 | 11 |
| 100 | 8 | 12 |
| 50 | 9 | 14 |

TABLE II
Optical Ground Station Locations for SYS 1

| Site | Lon. | Lat. | $P_{CFLOS}$ | $P_{owc}$ | Avail. |
|---|---|---|---|---|---|
| Zafarana | 32.6 | 28.8 | 92.24% | 0.00% | 92.244% |
| Yanbu | 37.6 | 24.2 | 86.86% | 84.08% | 98.765% |
| Jeddah | 39.2 | 21.6 | 86.88% | 75.58% | 99.699% |
| Gibraltar | −5.8 | 36.2 | 65.15% | 49.29% | 99.847% |
| Montpellier | 4.3 | 43.5 | 58.42% | 38.32% | 99.906% |

TABLE III
Optical Ground Station Locations for SYS 2

| Site | Lon. | Lat. | $P_{CFLOS}$ | $P_{owc}$ | Avail. |
|---|---|---|---|---|---|
| Nicosia | 33.4 | 34.8 | 79.31% | 0.00% | 79.311% |
| Gibraltar | −5.8 | 36.1 | 67.52% | 54.82% | 90.654% |
| Barcelona | 1.8 | 41.3 | 63.29% | 50.02% | 95.329% |
| Lausanne | 6.9 | 46.4 | 45.67% | 48.39% | 97.589% |
| Naples | 14.0 | 41.0 | 61.59% | 45.88% | 98.695% |
| Porto | −8.8 | 41.5 | 59.62% | 37.57% | 99.186% |
| Rennes | −2.1 | 48.1 | 39.55% | 35.79% | 99.477% |
| Tirana | 19.5 | 41.3 | 61.61% | 43.99% | 99.707% |
| Avila | −4.8 | 40.4 | 59.83% | 27.32% | 99.787% |
| Messina | 15.2 | 38.2 | 59.76% | 24.16% | 99.839% |
| Granada | −3.2 | 37.0 | 67.08% | 18.58% | 99.869% |
| Lisbon | −9.2 | 38.6 | 66.68% | 14.13% | 99.887% |
| Poitiers | 0.2 | 46.8 | 41.82% | 11.39% | 99.900% |
| Strasbourg | 7.2 | 47.5 | 34.54% | 8.57% | 99.909% |

TABLE IV
OPTICAL GROUND STATION LOCATIONS FOR SYS 3

| Site | Lon. | Lat. | $P_{CFLOS}$ | $P_{owc}$ | Avail. |
|---|---|---|---|---|---|
| Zafarana | 32.6 | 28.8 | 92.24% | 0.00% | 92.244% |
| Yanbu | 37.6 | 24.2 | 86.86% | 84.08% | 98.765% |
| Jeddah | 39.2 | 21.6 | 86.88% | 75.58% | 99.699% |
| Sevilla | –5.9 | 37.5 | 65.41% | 51.18% | 99.853% |
| Grenoble | 5.9 | 45.2 | 43.10% | 38.83% | 99.910% |

fact that only one OGS is activated at a time is called OGS fractional use.

The data transport between the INGs and the OGSs could be done either through optical fiber capacity leasing or through a deployed proprietary fiber network. Another simple option would be to pay for Internet access and create virtual private networks between the INGs and the OGSs. However, this option cannot meet the requirements of the service level of agreement: 1 Tbps of capacity, high availability (above 99.9%), and high quality of service. A second issue is raised because of the OGS fractional use. Indeed, it would be beneficial to lease the capacity when it is needed. However, no commercial offers match these requirements, and we believe that no wholesale carriers will accept this capacity fractional leasing and its frequency due to BATS specificities: some OGSs will be used less than 1% of the year, the OGS handover is not predictable in the long term, and the amount of necessary capacity for the links is huge (from several Gbps to 1 Tbps). As a consequence, only static leasing or proprietary networks were selected as potential solutions.

## B. Problem Modeling

The objective of this section is to find out the topology that minimizes the backbone cost based on the OGSN designed in Section II. The optimization is based on graph theory under the assumption that there is one PoP per country served by BATS, concentrating the entire traffic

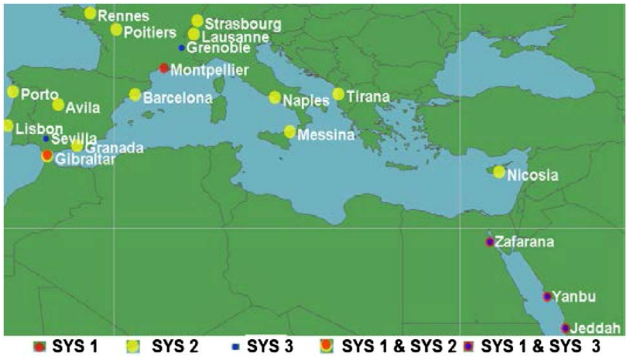


Fig. 6. Optimized OGSN function of the scenarios. The sites of SYS 1 correspond to the PoPs on the cheapest optical fibers of the extended pan-European network. The OGSs of SYS 2 are installed close to the PoPs of the pan-European network. SYS 3 is SYS 2 extended with submarine cables.

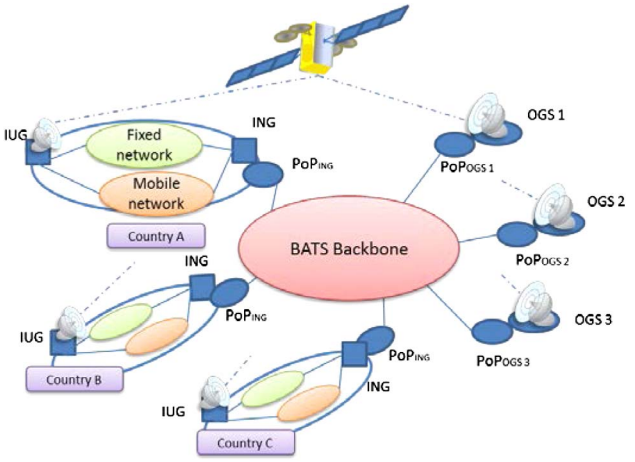


Fig. 7. Structure of the BATS network. The user has access through its IUG to three access networks: a national fixed provider, a national mobile provider, and a European satellite provider. An ING controls the IUGs, and it splits/combines/routes the traffic depending on the three link status and the required quality of experience. The backbone should connect the national ING to all the OGSs.

outgoing/incoming from/to this country. So, there are $N \times D$ flows between the $N$ OGSs and the $D$ INGs. Figure 8 depicts 1) the graph of the optical fibers used for the backbone optimization, 2) the 28 INGs ($D = 28$), and 3) the three optimized OGSNs (SYS1/SYS2/SYS3).

The graph was obtained by rejecting the unnecessary links to isolated or redundant PoPs of the full pan-European network illustrated in SYS 3 of Fig. 4. The same graph is considered from the backbone optimization of the three OGS networks.

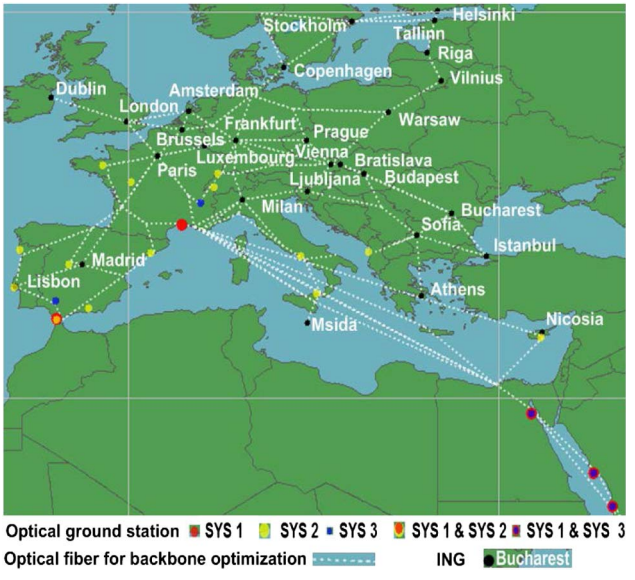


Fig. 8. ING locations for the 28 countries served by BATS plus the pan-European optical fiber graph for the backbone optimization. Each ING concentrates the traffic flows for its country.

### C. Cost Metric Definition

The optical fiber cost depends on numerous parameters:

- The capacity of the link: the price of the link increases as a function of the necessary capacity. Nevertheless, as the cost per Mbps diminishes with the data rate up to 10 Gbps, splitting the traffic of one ING into several paths is not interesting.
- The importance of the link: the cost of widely used fibers in the pan-European network is the least expensive due to a more competitive market between wholesale carriers.
- The type of the link: the price varies with the type of link. For instance, terrestrial fibers are usually less expensive than submarine cables.
- The wholesale carrier's price strategy: the price varies as a function of the firm.
- The distance: the price often increases with the distance; however, its impact is less than that of the four parameters above.

As there is only very little information publicly available from the wholesale carriers about the cost, it is impossible to derive a precise cost model. As a result, we propose a simple model in Eq. (1) where the cost of a link is composed of two terms. The first quantity, $\text{Cost}_{\text{static}}$, is the part of the cost that is independent of the link capacity (e.g., equipment and building fees). The second term is the cost of the requested capacity and is simply derived from the multiplication of the link capacity Capa(link) and an estimated cost $\text{Price}_{\text{Mbps}}$ (link) of \$1 per Mbps per month for all the links of the graph. The assumption behind the latter value is that at least one of the actors within the pan-European network presented in Section II will follow the market price decrease given in [23]. It has also been assumed that the submarine cable deployment from Europe to the Middle East between 2016 and 2020 [21] will lead to an important price drop and bring it to the order of magnitude of the terrestrial fiber cost. The required capacity for one link, Capa(link), is computed from Eq. (2). We select one $\text{OGS}_i$, and we sum all the necessary capacity for traffic $\text{Capa}(\text{s}, \text{OGS}_i, \text{link})$ between all the sources and the $\text{OGS}_i$ on the studied link. Then this operation is repeated for each OGS. Due to the OGS fractional use, the final required capacity for this link is only the maximum capacity among all the OGSs:

$$\text{Cost}(\text{link}) = \text{Cost}_{\text{static}} + \text{Price}_{\text{Mbps}}(\text{link}) \cdot \text{Capa}(\text{link}), \quad (1)$$

$$\text{Capa}(\text{link}) = \max_{\text{over OGS}} \left( \sum_{\text{s}=1}^{\text{D}} \text{Capa}(\text{s}, \text{OGS}_i, \text{link}) \right). \quad (2)$$

### D. Methodology

The backbone optimization is too complex to be solved with a brute-force algorithm because of the high amount of possible combinations. Even with harsh constraints, the minimal number of combinations exceeds $10^{40}$. Some heuristics must be developed to obtain an interesting solution in less than 1 h computation time. Common algorithms [24,25] were discarded due to the nonlinearity of Eq. (2). The innovative heuristic developed hereafter aims at reusing at most the same links for different OGSs; this target comes from the OGS fractional use specific to the optical feeder link. As a consequence, the heuristic relies on the observation that groups of OGSs and groups of data traffic sources (INGs) are not far from each other. Thus, each flow related to a source and an OGS that belongs to these groups may follow a similar optimized path, called a mutual path. In our graph, the vertices are interconnection points between several optical fibers (some of the PoPs). They can also be OGSs or/and INGs. The convergence vertices are the vertices at the start and the end of the mutual path, and each one is associated with a group. For instance, in Fig. 9, the sources 1, 2, and 3 can be gathered in group A and OGSs 7 and 8 in group B. The vertices 1 and 6 are convergence vertices, and the path [1,4,5,6] is the mutual path.

The optimization is split into three steps: 1) the selection of the best mutual paths between groups, 2) the optimization of local network topology within each group with respect to its convergence vertex, 3) the overall optimization that combines the results of the two previous steps.

In the first step, a pair of convergence vertices between two groups is selected such that it minimizes the cost of the network composed of the shortest path between each group and its corresponding convergence vertex plus the shortest path between the two convergence vertices. The metric used by the shortest path algorithm is Eq. (1). Equation (2) becomes linear from the group of sources to the OGS convergence vertex; it is equal to the sum of the INGs' capacities. We made the approximation that it is the same capacity computation that is applicable for the OGS group in order to have a linear equation to carry out the shortest path algorithm. The next step will overpass this approximation.

In a second step, a brute-force algorithm optimizes the cost of the local networks between the groups and their convergence vertices (e.g., between 6, 7, and 8 for the OGS group B) based on Eqs. (1) and (2).

The previous steps result in one or several mutual paths and local network topologies with equal minimum costs.

Thus, the last step consists of selecting the best combinations of these previous results to link each group of

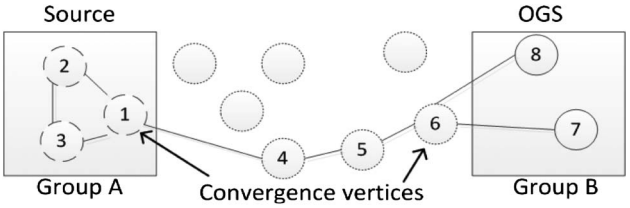


Fig. 9. BATS backbone optimization methodology. Vertices 1 and 6 are convergence vertices. Path [1,4,5,6] is the mutual path. Vertices {1,6} and the mutual path ensure the overall minimum cost that includes 1) the minimum cost between the sources of group A and vertex 1, 2) the minimum cost between the OGS of group B and vertex 6, and 3) the minimum cost of the mutual path.

sources to each group of OGSs. The algorithm is based on an iterative process. At each iteration, the metric in Eq. (3) below is recomputed for all the combinations related to unconnected pairs of groups. The selected combination is the one that maximizes the metric, and the pair of groups related to this combination is considered as connected. The algorithm stops when each OGS group is connected to each INGs group. The metric used is

$$\text{Metric(cmb)} = w_{\text{int}} \cdot L_{\text{int}}(\text{cmb}) + \frac{w_{p1}}{w_{p2} + p_{\text{add}}(\text{cmb})}. \quad (3)$$

The level of interest of a vertex is the number of times it is selected as an OGS, an ING, or a convergence vertex, or in an already selected path from previous iterations. The level of interest of a combination $L_{\text{int}}(\text{cmb})$ is the sum of the levels of interest of the vertices in each path of the combination. It reflects the potential of the path to be beneficial in the following iterations of the algorithm. The second term in Eq. (3) includes the additional cost of the new considered combination ($P_{\text{add}}(\text{cmb})$) derived from Eq. (1); it is the cost difference between the cost of the incomplete network, which is composed of the combinations selected during previous iterations, and the cost of this incomplete network plus the new combination. $w_{\text{int}}$, $w_{p1}$, and $w_{p2}$ are weights to ponder the level of interest with respect to additional combination prices.

### E. Results

The parameters of the BATS backbone cost optimization are given in Table V. The static price $C_{\text{static}}$ corresponds to the benchmark price of the public Internet exchange point. The weights in the metric in Eq. (3) have been thought in order to promote combinations with zero additional cost $P_{\text{add}}$. The term $w_{p2}$ avoids a zero division. $w_{\text{int}}$ and $w_{p1}$ have been defined in order to favor the combinations that add less than \$200/month to the total backbone price. Several runs have been carried out, and this order of magnitude gives the best results.

As a result, the applied methodology provides similar or better results in less than 5 min compared to a brute-force run of several days. Table VI presents the cost results for the BATS backbone considering the three OGSNs (SYS 1/SYS 2/SYS 3) optimized in Section II.

The overall cost of the backbone is estimated to be between 13 and 25 million dollars per month. The European system (SYS 2) is far more expensive than SYS 1 and SYS 3 due to a higher number of OGSs. SYS 1 is slightly better than SYS 3 due to more favorable positions of the OGSs.

TABLE V
BATS Backbone Topology and Cost Optimization Parameters

| Parameter | Value |
|---|---|
| $C_{\text{static}}$ [\$] | 10,000 |
| $\text{price}_{\text{Mbps}}$[\$/Mbps] | 1 |
| $w_{\text{int}}$ | 1 |
| $w_{p1}$ | 20,000 |
| $w_{p2}$ | 0.0001 |

TABLE VI
BATS Backbone Topology and Cost Optimization Results

| SYS | Pool of PoP | Overall Rental Cost (k\$/month) |
|---|---|---|
| 1 | Cheaper extended pan-European | 13,100 |
| 2 | All pan-European | 25,300 |
| 3 | All extended pan-European | 14,000 |

Despite the uncertainty on the cost model, the order of magnitude of the backbone cost emphasizes the importance of its optimization. The increase of the backbone expense with the number of OGSs reinforces our approach of merging OGS positioning and backbone optimizations. Also, there is great interest in extending the potential OGS locations to Africa and the Middle East; however, this improvement may be jeopardized by a higher price of the necessary submarine cables. If the submarine cable price decreases in a smaller extension than expected, then the cost trade-off between the three scenarios needs to be revised.

Moreover, capacity leasing does not seem appropriate for such a high-capacity backbone, and using proprietary fibers appears to be the preferable solution. With this idea in mind, a rough estimation for the deployment of a 1 Tbps fiber over high-voltage power lines between Sevilla and Lisbon has been requested from a terrestrial fiber operator. The deployment of such fiber is ~37 times less expensive than the renting cost. If proprietary fibers are assumed, the cost function should be updated, taking into consideration the length of the fibers that need to be deployed. Despite this modification, the heuristic developed for the backbone optimization would still be applicable. Independent from the cost model, innovative solutions could be envisaged to lower the cost of the BATS backbone:

- Renting the unused capacity: the entire capacity is not permanently used in this network and could be sold through a new data transit agreement.
- Defining specific service level agreements for users: the less-used OGSs will provide a lower throughput to some users and high throughput only to prior users during a small percentage of the year.

## IV. Satellite System Architecture and Concept of Operation

In the previous sections, sets of OGSs were optimized in the vicinity of the ingress and egress points of real fiber networks to lower the overall cost of the system while reaching over 99.9% availability for the feeder link. A satellite operator backbone topology has been designed in the frame of a BATS project to limit its expense. The following section presents the generic laser link system architecture to mitigate cloud blockage and to lower the end-user

service interruption during a handover between two OGSs (i.e., the transfer of the data traffic from one OGS to another).

### A. Satellite System Architecture for Site Diversity

Figure 10 illustrates the system architecture for site diversity. The site diversity control center (SDCC) predicts the line-of-sight (LOS) status of the OGS sites and deduces the active OGS site. The feeder control center (FCC) operates the satellite operator backbone; in particular, it is in charge of routing the traffic for transfer from one OGS site to another. The satellite control center (SCC) operates the satellite. Two optical terminals (OTs) are installed on board the satellite to minimize the end-user service interruption: OT1 is the active OT; OT2 is the passive OT, used to acquire the next site in the case that a cloud blockage is foreseen over the active site. OT2 acquires the next OGS while OT1 is still communicating with the current site. The acquisition strategy is analogous to the one tested and proven during the Semiconductor Intersatellite Link Experiment (SILEX) campaign [26]. A bright and wide beacon confers robustness to the acquisition process. The beacon is implemented on the ground to simplify the satellite design and because more power is available at the ground station. The beacon wavelength is 1.55 μm for several reasons. First, as only one wavelength range is accommodated inside the terminals, chromatism effects on pointing and propagation errors are limited. Second, a 1.55 μm wavelength is well adapted to propagation through the atmosphere and is more eye safe than other, shorter telecom wavelengths [27].

### B. Line-of-Sight Cloud Blockage Prediction

In recent years, local cloud imager prototypes have been developed in the USA, Europe, and Japan [28–31]. The most interesting cloud detection system is the Infrared Cloud Imager (ICI) [30]. During the day and night, the ICI measures the cloud radiance (filtered in the [7.5–13.5] μm spectral band) within a field of view up to 110 deg. From these images, optical attenuation maps centered on the LOS with an ~1 dB power resolution are derived every 5 min. Then, intrahour cloud blockage forecasting can be performed from these attenuation map time series [32]. A similar approach based on cloud masks from satellite imagery was operationally demonstrated in 2014 [33]. The correlation between a cloud forecast and the truth is ~0.97 at 30 min [34]. Extension of the duration is possible with satellite imagery and numerical weather prediction (NWP) data, but at the price of higher uncertainty depending on the weather conditions and the surroundings. Nevertheless, it has been shown in a previous study that 6 h cloud forecasting is desirable in Europe, as it minimizes the number of handovers [11].

### C. Site Diversity Concept of Operation

The SDCC gathers the cloud attenuation maps every 5 min from the cloud imagers installed at all the OGSs. Considering the accuracy of the cloud forecast developed in [34], we assumed that the SDCC predicts cloud blockage events from these attenuation maps over 30 min. When a cloud obstruction is foreseen on an active OGS, it selects the next active OGS site that maximizes the CFLOS duration in the future and had the highest probability of CFLOS in the past. The handover process embraces the anticipation of cloud blockage, the selection of the next active site, the preparation of the physical and networks layers, and the execution of the switch. Its duration, noted as X in Fig. 11, is driven by the time necessary to prepare the physical and network layers. The preparation of the network layer is out of the scope of this paper because the position of the satellite operator modems has not been defined yet. The duration of the physical layer preparation is determined by the acquisition of the next site by OT2, whose maximal duration based on SILEX heritage is below 10 s.

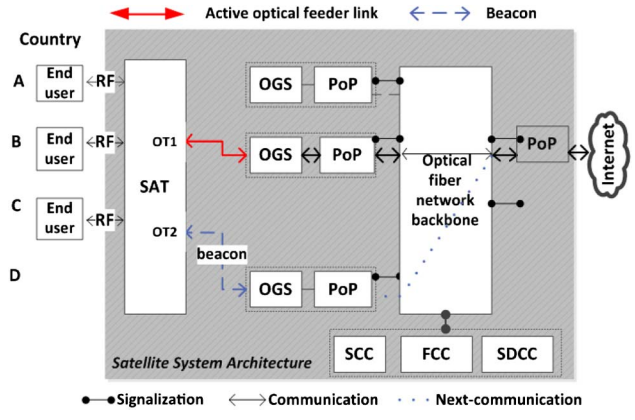


Fig. 10. Satellite system architecture for cloud blockage mitigation. The SDCC monitors the OGS's line of sight, selects the next site, and commands its acquisition. The FCC operates the backbone. The SCC operates the satellite.

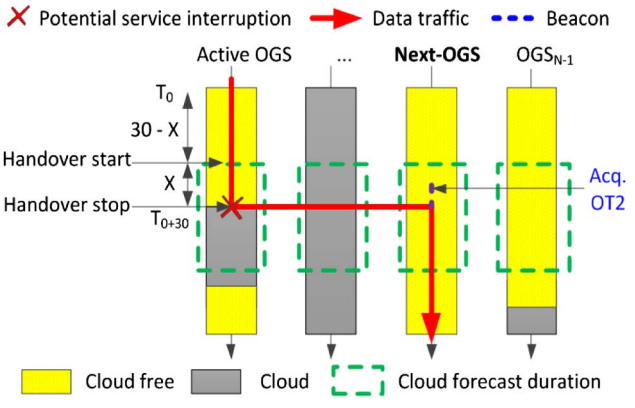


Fig. 11. Handover process description. The handover process is run in parallel with the communication with the active site. Handover duration X encroaches on cloud imagers forecasting durations (30 min). Service interruption could occur at the switch.

Handover execution could lead to service interruption due to loss of synchronization at physical and/or network layers. These service interruptions shall be taken into consideration in the computation of the availability.

## V. Performance

In the following, the feeder link availability is simulated step by step with the cloud mask data bank, taking into consideration a realistic concept of operation as defined previously. The simulation starts January 1 with an arbitrary active site and ends December 31 of the same year. When the active site becomes cloud blocked, the next active site is the one with the longest CFLOS forecast (forecast duration is either 30 min or 6 h) and that had the lowest probability of clouds in the past. The number of handovers over the year and the time intervals between successive handovers are stored during the simulation. As mentioned earlier, it is assumed that one active OGS can handle the terabit/second satellite capacity and that optical transmission through thin ice clouds is allowed by the optical link budget. Figure 12 depicts the average monthly optical feeder link availability for the three optimized OGSNs (SYS 1/2/3) over 2010–2011. The error bars correspond to half of the availability difference between 2010 and 2011; they provide the deviation between the two years. The average link availability is 99.906% for SYS 1, 99.909% for SYS 2, and 99.910% for SYS 3. It can be seen that the average monthly availability varies between 99.74% and 100%. The monthly availability deviation between the two years stays below 0.1%, except in September due to very bad weather conditions in 2011.

Short service interruptions during the handover could be tolerable only if their cumulative duration over a year does not exceed the link availability margin above the requirement. Assuming that these service interruptions during handover have a constant length of time, the cumulative duration is fully determined by the number of handovers, and hence by the cloud forecast duration. Two cases were simulated. For the first case, the cloud blockage prediction is based on local cloud imagers and the forecast duration is 30 min, equivalent to 2 cloud masks. For the second case, a new system gathering local cloud imagers, satellite imagery, and NWP data providing a cloud forecast over 6 h is considered. As is shown in Table VII, the average number of handovers per year for the OGSN of SYS 2 is 827/481 if the selection of the next OGS is done with a 30 min/6 h cloud forecast duration. With OGSs in Africa and the Middle East, the number of handovers is 254/202 for SYS 1 and 259/206 for SYS 3. Figure 13 provides the monthly distribution of handovers; it can be seen that these are much more frequent during winter and spring.

TABLE VII
Optical Ground Station Network Performance

| SYS | Average Handovers/ Year (30 min) | Average Handovers/ Year (6 h) | Average Link Availability/ Year (%) |
|---|---|---|---|
| 1 | 254 | 202 | 99.906 |
| 2 | 827 | 481 | 99.909 |
| 3 | 259 | 206 | 99.910 |

From the average number of handovers per year and the link availability results, the tolerable service interruption duration as a function of the targeted link availability, either 99.9% or 99.7%, is derived in Table VIII. When the required link availability is 99.9%, the previously optimized OGS networks allow only very short service interruption (between 3 and 16 s) due to the small availability margin. On the other hand, if the required link availability is reduced to 99.7%, service interruption from 1 to 5 min would be tolerable from a link availability point of view. In order to lower the impact of such service interruption on the end-user quality of experience, the time span between handovers should be maximized. To do so, Fig. 14, showing the cumulative distribution function of the length of time between successive handovers, highlights that a 6 h cloud forecasting system is highly preferable in Europe.

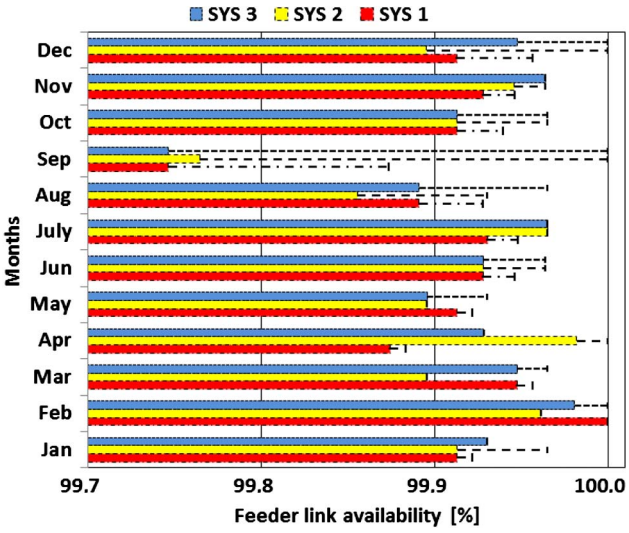


Fig. 12. Average monthly feeder link availability for the three optimized optical ground station networks.

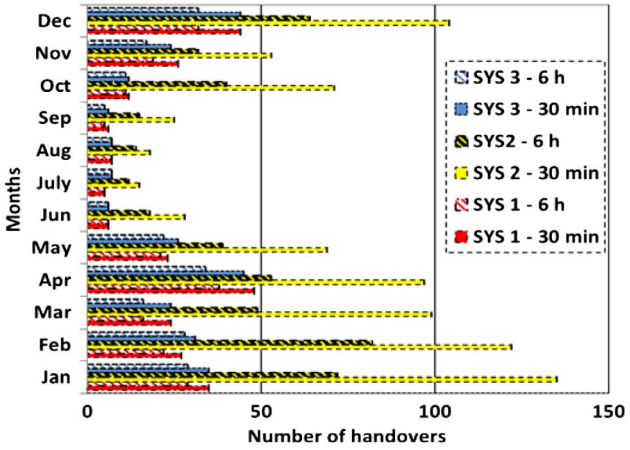


Fig. 13. Average number of handovers for three optimized ground station networks as a function of cloud forecasting duration.

TABLE VIII
TOLERABLE SERVICE INTERRUPTION AS A FUNCTION OF AVAILABILITY REQUIREMENTS AND CLOUD FORECAST DURATION

| SYS | At 99.9% (30 min) | At 99.9% (6 h) | At 99.7% (30 min) | At 99.7% (6 h) |
|---|---|---|---|---|
| 1 | 7 s | 9 s | 4 min | 5 min |
| 2 | 3 s | 6 s | 1 min | 2 min |
| 3 | 12 s | 16 s | 4 min | 5 min |

The last outcome, depicted in Fig. 15, is the simulated utilization of the $N$ OGSs in 2011, considering the algorithm of the selection of the next OGS as well as the cloud forecasting system defined in Subsection IV.C. As a result, 90% of the traffic is concentrated between two OGSs for SYS 1 and SYS 3 and between 9 OGSs for SYS 2.

Considering the distribution of OGS utilization as well as the specific backbones designed for the BATS project

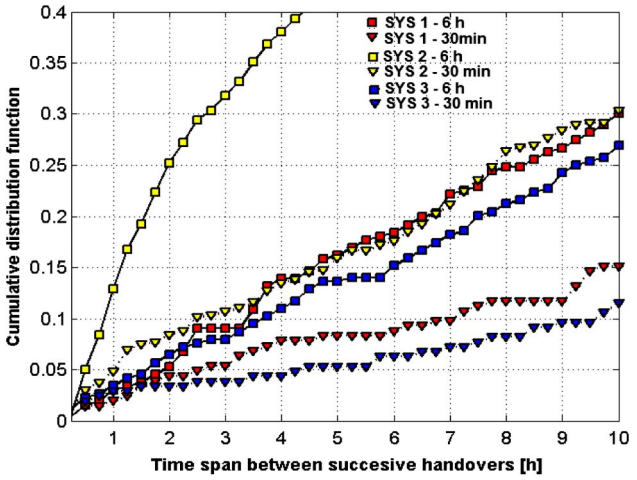


Fig. 14. Cumulative distribution function of the time span between successive handovers, computed over the two years 2010 and 2011.

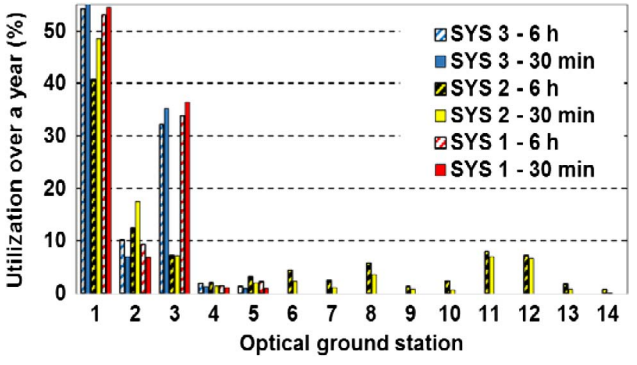


Fig. 15. Distribution of the OGS utilization over a year for each network. Use of OGS 3 takes priority when OGS 1 is cloud blocked, because its probability of CFLOS (in the past) is higher than OGS 2. In Europe (SYS 2), the utilization distribution is more homogeneous over OGS 2–OGS 14.

TABLE IX
BATS BACKBONE AVERAGE UNUSED RENTED CAPACITY PER YEAR

| SYS | Rented Capacity [Gbps/year] | Unused Capacity [%/year] |
|---|---|---|
| 1 | 12,600 | 59% |
| 2 | 24,625 | 74% |
| 3 | 13,700 | 62% |

in Section III, the unused rented capacity is evaluated in Table IX.

The inefficient usage of the BATS operator backbone is striking. Indeed, for SYS 1 and SYS 3, over half of the rented capacity is unused, and that increases up to 74% for SYS 2. The higher percentage of unused backbone for SYS 2 is due to a bigger OGSN compared to SYS 1 and SYS 3. The huge cost of the BATS backbone encourages the consideration of a new business case to increase the profitability of the network. For instance, the unused BATS backbone capacity could be leased in the frame of an innovative business model.

## VI. CONCLUSION

In the present paper, we addressed for the first time (to our knowledge) the design of the satellite operator ground segment for a terabit/s optical feeder link from a satellite system point of view. To design a cost-effective ground segment, we proposed a new method in two steps aiming at a joint optimization of the OGS positioning and the satellite operator backbone. The innovation consists of constraining the OGS positioning around the ingress and egress points of the optical fiber networks considered during the backbone optimization. A lot of attention was also paid to providing a realistic model of the optical feeder link system, 1) by taking into consideration existing or planned high-data-rate optical fiber networks, 2) by evaluating the feeder link availability from a state-of-the-art cloud mask detecting high-altitude ice clouds (cirrus), and 3) by simulating two full years of OGSN operation, considering a practical cloud blockage forecasting system capability.

The OGS positioning was performed with an iterative greedy optimization process based on conditional opposite weather conditions and stopped when the 99.9% feeder link availability specified by the satellite operator was reached. It was found that at least nine OGSs are necessary in Europe, and up to 14 are required if the OGS must be installed less than 50 km from existing egress and ingress points of the optical fiber network. Moreover, we found two compliant five-OGS networks by taking advantage of the short-term availability of submarine cables with 1 Tbit/s capacity. It has also been demonstrated that the last remaining percentage of optical feeder link availability is very demanding in terms of the number of OGSs, and this fact strengthens the motivation to propose new broadband service with a lower level of availability. With this idea in mind and from the satellite operator

specifications, a feeder link availability of 99.7% was also studied and led to very interesting results. Indeed, the 0.2% of extra availability could be used to reduce the size of the OGSN (respectively for the two previously stated cases, from 14 to 8 and from 5 to 3) or to eliminate one OT on board the satellite.

Our new method for satellite operator ground segment optimization was already applied in a concrete case of study (the BATS project) assuming optical fiber leasing. Thanks to our method, we optimized a realistic backbone topology for a terabit/second satellite system. The design of the backbone was performed according to graph theory, and a specific heuristic was defined for this case of study. We performed as well a first assignment of the backbone cost.

In the future, our joint optimization method will be applied, taking into consideration a proprietary cost model. In addition, the OGS positioning optimization will take into consideration the atmospheric turbulence [35] that impacts very-high-data-rate optical communications.

## Acknowledgments

This work was supported in part by the European Commission FP7 program in the frame of the research project BATS (Broadband Access via integrated Terrestrial and Satellite systems).

## References

[1] European Commission, "A digital agenda for Europe," Aug. 26, 2010 [Online]. Available: http://ec.europa.eu/digital-agenda/en/digital-agenda-europe-key-publications.

[2] Point Topic, "Mapping is vital to broadband investment," 2011 [Online]. Available: http://point-topic.com/press-and-events/2011/mapping-is-vital-to-future-broadband-investment-2/.

[3] G. Verelst, O. Vidal, E. Albert, D. Galinier, N. Metzger, and P. Inigo, "Innovative system architecture to reach the terabit/s satellite," in *31st AIAA Int. Communications Satellite Systems Conf.*, 2013, pp. 45–52.

[4] J. Pérez-Trufero, B. Evans, A. Kyrgiazos, M. Dervin, B. Garnier, and C. Baudoin, "High throughput satellite system with Q/V band gateways and its integration with terrestrial broadband communication networks," in *32nd AIAA Int. Communications Satellite Systems Conf.*, 2014, pp. 255–264.

[5] E. Ciaramella, Y. Arimoto, G. Contestabile, M. Presi, A. D'Errico, V. Guarino, and M. Matsumoto, "1.28 terabit/s WDM transmission system for free space optical communications," *IEEE J. Sel. Areas Commun.*, vol. 29, pp. 1639–1645, 2009.

[6] F. Moll and M. Knapek, "Wavelength selection criteria and link availability due to cloud coverage statistics and attenuation affecting satellite, aerial, and downlink scenarios," *Proc. SPIE*, vol. 6709, 670916, 2007.

[7] G. S. Wojcik, H. L. Szymczak, R. J. Alliss, R. P. Link, M. E. Craddock, and M. L. Mason, "Deep-space to ground laser communications in a cloudy world," *Proc. SPIE*, vol. 5892, 589203, 2005.

[8] F. Lacoste, A. Guérin, A. Laurens, G. Azema, C. Périard, and D. Grimal, "FSO ground network optimization and analysis considering the influence of clouds," in *Proc. EUCAP*, 2011, pp. 2746–2750.

[9] Y. Takayama, M. Toyoshima, and N. Kura, "Estimation of accessible probability in a low earth orbit satellite to ground laser communications," *Radioengineering*, vol. 19, pp. 249–253, 2010.

[10] E. Lutz, "Achieving a terabit/s geo satellite system," in *19th Ka and Broadband Communications, Navigation and Earth Observation Conf.*, Florence, Italy, 2013.

[11] Community Research and Development Information Service of European Commission, "Broadband Access via integrated Terrestrial and Satellite systems," Feb. 2013 [Online]. Available: http://cordis.europa.eu/fp7/ict/future-networks/documents/call8-projects/bats-factsheet.pdf.

[12] S. Poulenard, B. Roy, M. Hanna, F. Lacoste, H. Le Gléau, and A. Rissons, "Optical ground network optimization and performances for high data rate geosatellite-to-ground telemetry," in *Proc 6th ESA Int. Workshop on Tracking, Telemetry and Command Systems for Space Applications*, 2013.

[13] J. Schmetz, P. Pili, S. Tjemkes, D. Just, J. Kerkmann, S. Rota, and A. Ratier, "An introduction to Meteosat Second Generation," *Bull. Am. Meteorol. Soc.*, vol. 83, pp. 977–992, 2002.

[14] M. Derrien, H. Le Gléau, and P. Fernandez, "Validation Report for 'Cloud Products' (CMa-PGE01 v3.2, CT-PGE02 v2.2 & CTTH-PGE03 v2.2)," NWC SAF, Tech. Rep., 2012, http://www.nwcsaf.org/scidocs/Documentation/SAF-NWC-CDOP-MFL-SCI-VR-06_v1.0.pdf.

[15] S. Poulenard, M. Ruellan, B. Roy, J. Riédi, F. Parol, and A. Rissons, "High altitude clouds impacts on the design of optical feeder link and optical ground station network for future broadband satellite services," *Proc. SPIE*, vol. 8971, 897107, 2014.

[16] L. Andrews and R. Phillips, *Laser Beam Propagation Through Random Media*. SPIE, 2005.

[17] European Internet Exchange Association, "European Internet Exchange point list of Euro-IX" [Online]. Available: https://www.euro-ix.net/ixp-member-list.

[18] Level 3 optical fiber network, 2015 [Online]. Available: http://www.level3.com/~/media/files/maps/map_1014_interactive.pdf.

[19] Cogent optical fiber network, 2015 [Online]. Available: http://www.cogentco.com/files/images/network/network_map/networkmap_global_large.png.

[20] Interoute optical fiber network, 2015 [Online]. Available: http://www.interoute.com/our-network.

[21] TeleGeography Submarine cable optical fiber map, 2014 [Online]. Available: http://www.submarinecablemap.com.

[22] D. Wylie, D. L. Jackson, W. P. Menzel, and J. J. Bates, "Trends in global cloud cover in two decades of HIRS observations," *Bull. Am. Meteorol. Soc.*, vol. 18, pp. 3021–3031, 2005.

[23] Telegeography IP transit price, 2014 [Online]. Available: https://www.telegeography.com/products/commsupdate/articles/2014/09/24/ip-transit-price-declines-slow-globally/.

[24] H. N. Nguyen, D. Habibi, V. Q. Phung, S. Lachowicz, K. Lo, and B. Kang, "QRP02-5: Joint optimization in capacity design of networks with p-cycle using the fundamental cycle set," in *IEEE Global Telecommunications Conf.*, 2006.

[25] N. G. Chattopadhyay, T. W. Morgan, and A. Raghuram, "An innovative technique for backbone network design," *IEEE Trans. Syst. Man Cybern.*, vol. 19, no. 5, pp. 1122–1132, Sept./Oct. 1989.

[26] G. Planche and V. Chorvalli, "SILEX in-orbit performances," in *Proc. 5th Int. Conf. on Space Optics*, 2004, pp. 403–410.

[27] "Safety of laser products—Part 1: Equipment classification and requirements," European standard EN 60825-1, p. 43, Table 4, 2007 [Online]. Available: http://www.bristol.ac.uk/media-library/sites/nsqi-centre/documents/lasersafetybs.pdf.

[28] M. Toyoshima, Y. Munemasa, H. Takenaka, Y. Takayama, Y. Koyama, H. Kunimori, T. Kubooka, K. Suzuki, S. Yamamoto, S. Taira, H. Tsuji, I. Nakazawa, and M. Akioka, "Introduction of a terrestrial free-space optical communications network facility: IN-orbit and Networked Optical ground stations experimental Verification Advanced testbed (INNOVA)," *Proc. SPIE*, vol. 8971, 89710R, 2014.

[29] J. E. Shields, M. E. Karrn, R. W. Johnson, and R. A. Burden, "Day/night whole sky imagers for 24-h cloud and sky assessment: History and overview," *Appl. Opt.*, vol. 52, no. 8, pp. 1605–1616, 2013.

[30] P. W. Nugent, J. A. Shaw, and S. Piazzolla, "Infrared Cloud Imager development for atmospheric optical communication characterization, and measurements at the JPL Table Mountain Facility," IPN Progress Report 42-192, 2013.

[31] Y. Gonzalez, C. López, and E. Cuevas, "Automatic observation of cloudiness: Analysis of all-sky images," in *World Meteorological Organization Technical Conf.*, Brussels, Belgium, Oct. 2012.

[32] C. W. Chow, B. Urquhart, M. Lave, A. Dominguez, J. Kleissl, J. Shields, and B. Washom, "Intra-hour forecasting with a total sky imager at the UC San Diego solar energy testbed," *Sol. Energy*, vol. 85, no. 11, pp. 2881–2893, 2011.

[33] R. J. Alliss and B. Felton, "Realtime atmospheric decision aids in support of the lunar laser communications demonstration," in *Proc. Int. Conf. on Space Optical Systems and Applications (ICSOS)*, 2014.

[34] Consultative Committee for Space Data System, "Green book concerning real-time weather and atmospheric characterization data," 2014 [Online]. Available: http://cwe.ccsds.org/sls/docs/Forms/.

[35] S. Cheinet, K. Weiss-Wrana, Y. Hurtaud, and A. Beljaars, "Global prediction of the optical sensing through turbulence," *Proc. SPIE*, vol. 7828, 782806, 2010.

**Sylvain Poulenard** received his Master of Engineering from the French graduate engineering school TELECOM Bretagne in 2011. Since 2012, he has been doing research for Airbus Defence and Space in cooperation with the Institut Supérieur de l'Aéronautique et de l'Espace (ISAE) in order to earn his Ph.D. degree. His research interests include system design of space-to-ground bidirectional optical links and satellite systems.

**Michael Crosnier** received an M.Sc. degree in telecommunication and networks engineering and an M.S. degree in telecommunication researching, both from the National Polytechnic Institute of Toulouse in France in 2009, and a Ph.D. degree in computing and telecommunication from the National Polytechnic Institute of Toulouse and the University of Toulouse in France in 2013. Since 2013, he has been working at Airbus Defence and Space as a satellite system engineer. His research interests include system design of hybrid satellite/terrestrial networks.

**Angelique Rissons** received an M.S. degree in microwave and optoelectronics and a Ph.D. degree from the The French Grande Ecole Supaero (National School of Aeronautics and Space), Toulouse, France, in 2000 and 2003, respectively. Her doctoral thesis concerned the opto-microwave modeling 850 nm VCSEL for data communication. In 2004, she joined Institut Supérieur de l'Aéronautique et de l'Espace (ISAE), Toulouse, France, as an associate professor. She is in charge of the Microwave-Photonics of the Department of Electronics-Optronics-Signals (DEOS). She worked on the 1550 VCSEL modeling for telecom applications and microwave signal generation by using optical functions (optoelectronic oscillator, optical injection locking). In 2012, she became a professor at ISAE. Her research interests include photonics space applications and space-to-ground optical communication.